
# Energy balance analysis of a propeller in open water

Ocean Engineering 158 (2018) 162–170

Contents lists available at ScienceDirect

Ocean Engineering

journal homepage: www.elsevier.com/locate/oceaneng

# Energy balance analysis of a propeller in open water

Jennie Andersson [a,*], Arash Eslamdoost [a], Alexandre Capitao Patrao [a], Marko Hyensjö [b], Rickard E. Bensow [a]

[a] Chalmers University of Technology, Department of Mechanics and Maritime Sciences, 412 96, Göteborg, Sweden
[b] Rolls-Royce Hydrodynamic Research Centre, Rolls-Royce AB, Kristinehamn, Sweden

ARTICLE INFO

*Keywords:*
RANS
Propeller in open water
Reynolds transport theorem
Energy balance
Hydrodynamic losses

ABSTRACT

This paper proposes a methodology based on control volume analysis of energy, applied on Computational Fluid Dynamics (CFD) results, for analyzing ship propulsion interaction effects as a complement to the well-established terminology, including thrust deduction, wake fraction and propulsive efficiency. The method, titled *Energy Balance Analysis*, is demonstrated on a propeller operating in open water. Through consideration of a complete energy balance, including kinetic energy flux, turbulent kinetic energy flux, internal energy flux (originating from dissipation) and pressure work, all possible hydrodynamic losses are included in the analysis, implying that it should be possible to avoid sub-optimized solutions. The results for different control volumes and grid refinements are compared. The deviation of the power obtained from the proposed energy balance analysis relative to the power based on integrated forces on the propeller is less than 1%. The method is considered promising for analyzing and understanding propulsor hull interaction for conventional, as well as novel propulsion configurations. The energy balance analysis is conducted as a post-processing step and could be used in automated optimization procedures.

## 1. Introduction

The interaction effects between hull and propulsion system are most commonly described using a well-established terminology, including thrust deduction, wake fraction, propulsive efficiency etc. However this decomposition has its primary origin in the experimental procedures used to establish ship scale performance rather than from principles of hydrodynamics. This can imply limitations in design and optimization of hull and propulsion system, as the interaction may thus not be correctly represented. We believe that the reliability and capacity of modern Computational Fluid Dynamics (CFD) has reached a high level of maturity which can be used to extract detailed data of the flow around vessels and propulsion units, even in full scale.

Different methods for analyzing interaction effects based on CFD or other calculated results have been proposed in the literature. Dyne (1995) suggested a propulsive efficiency based on wake losses and gains. The method was derived based on potential flow assumptions, which implies that it is not applicable for analyzing viscous flow simulation results. However, it is an appealing idea and easily understandable concept to separate the flow features in losses and gains. Dang et al. (2012, 2015) evaluated the dimensionless kinetic energy in the wake for comparison of different propulsion systems. This methodology focuses on axial and transverse kinetic energy, without accounting for all the energy transferred from the propeller to the water. A more comprehensive methodology was proposed by van Terwisga (2013) based on an energy balance over a control volume enclosing the entire vessel including propulsion unit. Through the assumption of a uniform control volume inflow, the evaluation of the fluxes were limited to the control volume downstream boundary. However, the method was not demonstrated. Schuiling and van Terwisga (2016) suggested a methodology for performing an energy analysis based on evaluation of the energy equation over a control volume, and applied it on a propeller operating in open water. The viscous losses are obtained through volume integrals of the dissipation terms. Thus, the numerical dissipation, which cannot be evaluated from CFD, has to be obtained indirectly from the difference between delivered power, obtained from forces acting on the propeller, and the other energy components.

Interaction effects and wake analyses has also been studied within the aircraft industry, using control volume analyses of energy, for instance by Denton (1993), Drela (2009) and Capitao Patrao et al. (2016). Designers developing novel aircraft concepts, such as Boundary Layer Ingestion (BLI), are actually facing very similar design issues as ship propulsion

* Corresponding author.
*E-mail address:* jennie.andersson@chalmers.se (J. Andersson).

https://doi.org/10.1016/j.oceaneng.2018.03.067
Received 10 November 2017; Received in revised form 16 February 2018; Accepted 26 March 2018

system designers, with propulsion units operating in the wake of the craft.

The objective of this paper is to propose a methodology based on control volume analysis of the energy equation for analyzing ship propulsion interaction effects. Unlike other proposed methods for hull propulsion system interaction the energy equation is solved, which provides a clearer picture of the hydrodynamic losses caused by dissipation of kinetic energy. The method will be demonstrated on a simplified case, a propeller operating in open water.

## 2. Energy balance method

The methodology is based on the evaluation of the energy equation over a control volume surrounding the propulsion system, with the flow field obtained through CFD. It will be possible to express the delivered power, which traditionally is evaluated through the torque acting on the blades, as a sum of energy fluxes through the control volume surface. The reason for selecting energy, and not momentum, for the control volume analysis is described by van Terwisga (2013). As long as a ship moves at a steady speed, for a control volume enclosing the entire ship with propeller, no net momentum change in the flow exists whereas an energy change over the control volume can be measured. Thus, all effects of a new design, which appear in form of different energy losses in the flow, can be identified by means of studying the energy change through the control volume.

Control volume analyses, i.e. application of Reynolds Transport Theorem, is a well established tool, but has traditionally not been applied on CFD simulation results. Reynolds transport theorem states that *the change of any fluid property within the system is the sum of the change within the control volume, plus the outflow from the control volume, minus the inflow to the control volume*. The control volume could be of arbitrary shape, which is of importance to facilitate analyses of various kind of propulsion systems. Fig. 1 illustrates a possible control volume surrounding skeg, propeller and rudder. The control volume is bounded by both the virtual control volume surface (shown in blue), as well as the material surfaces, i.e. some proportion of the hull, the rudder and the propeller surfaces. To establish an energy balance accounting for all propulsive energy, the propulsion unit needs to be fully enclosed by the control volume. Selection of an appropriate control volume for the analyses will be further discussed in Section 4.

The energy conservation equation reads (White, 2008);

$$\Delta E = \dot{Q} - \dot{W}, \tag{1}$$

where $E$ represents energy, $\dot{Q}$ denotes the rate at which heat is added to the system and $\dot{W}$ denotes the rate at which work is done by the system. Heat transfer from ship and propulsion unit to surrounding water is neglected for these analyses, since associated energy fluxes do not contribute to the hydrodynamic analyses. For simplicity we describe a stationary system, i.e. a steady state or periodic unsteady flow, it is however possible to generalize the method for analyzing unsteady flows as well. Denoting energy per unit mass with $e$, the energy conservation equation without heat transfer using the Reynolds Transport Theorem for stationary flow yields (White, 2008),

$$\Delta E = -\dot{W} = \int_{CS} e\rho\left(\vec{V}\cdot\vec{n}\right)dA, \tag{2}$$

where $CS$ denotes the control volume surface, $\vec{V}$ the velocity vector, $\rho$ density and $\vec{n}$ the normal vector to the control volume surface (positive outwards). Note, for a periodic unsteady flow, the energy balance analysis needs to be evaluated as time-average over at least one period. The work done by the system constitutes work done by pressure and shear stresses on the control volume surface,

$$\dot{W} = \dot{W}_p + \dot{W}_v = \int_{CS}\left(p\left(\vec{V}\cdot\vec{n}\right) - \vec{\tau}\cdot\vec{V}\right)dA, \tag{3}$$

where $p$ denotes pressure and $\vec{\tau}$ is the shear stress vector on the elemental surface $dA$. The pressure and shear stress work acting on the rotating material surfaces of $CS$ constitutes the delivered power ($P_D$) and can be expressed as,

$$P_D = 2\pi nM, \tag{4}$$

where $M$ is the torque evaluated over all rotating material surfaces in $CS$ and $n$ denotes rotation rate. Compared to the classical notation, as shown in Eq. (1), the delivered power is here defined as power added to the system.

The pressure and shear stress work (Eq. (3)) also act on the virtual control volume boundaries of $CS$; these terms are moved to the right hand side of Eq. (2) and evaluated together with the energy fluxes. The work done by shear stresses on virtual boundaries of the control volume ($\dot{W}_{v,virtual}$) can often be neglected, this will be further examined in Section 4.1. Due to no-slip and no flux protruding the hull, no work is done by the system on the material surfaces in $CS$ fixed relative to the control volume.

To increase the level of detail in the energy balance, the energy per unit mass ($e$), occurring on the right hand side of Eq. (2), could be further decomposed. It is proposed to split the term into kinetic energy in axial direction, kinetic energy in transverse directions, internal energy and turbulent kinetic energy:

$$e = \frac{1}{2}V_x^2 + \frac{1}{2}\left(V_t^2 + V_r^2\right) + \hat{u} + k, \tag{5}$$

where tangential and radial velocity components are denoted by $V_t$ and $V_r$, respectively. In a Cartesian coordinate system these components should be replaced with the non-axial velocity components $V_y$ and $V_z$. Introducing Eq. (5) and the above mentioned decomposition of the work rate into Eq. (2), we obtain:

$$P_D = \int_{CS}\left(\frac{p}{\rho} + \frac{1}{2}V_x^2 + \frac{1}{2}\left(V_t^2 + V_r^2\right) + \hat{u} + k\right)\left(\vec{V}\cdot\vec{n}\right)dA + \dot{W}_{v,virtual}. \tag{6}$$

The presented approach, referred to as energy balance analysis in the rest of this paper, will be employed for the evaluation of a propeller

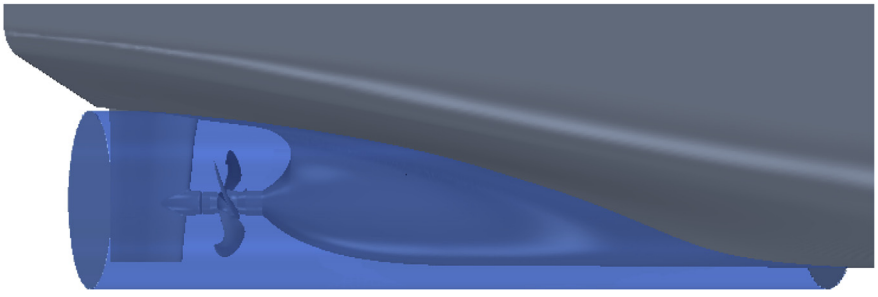

**Fig. 1.** Cylindrical control volume (in blue) surrounding skeg, propeller and rudder. (For interpretation of the references to color in this figure legend, the reader is referred to the Web version of this article.)

performance in open water in Section 4. Prior to this, the different terms which appear in Eq. (6) are discussed in Section 2.1–2.3.

### 2.1. Pressure work and axial kinetic energy flux

The propulsion unit is converting rotational motion to thrust. A pressure difference is produced between the forward and rear surfaces of the blade and the water is accelerated downstream. Accelerating water in any direction other than the course of the vessel will not contribute to useful thrust. To be able to distinguish between kinetic energy in preferred and non-preferred directions, it is beneficial to define the coordinate system so that the axial direction is in line with the vessels sailing direction, not necessary identical to the propeller axis. The kinetic energy flux in the preferred direction of motion for the ship is therefore denoted as *axial*.

As described by the actuator-disc model of a propeller, low and high pressure regions are generated ahead and behind the propeller disk, respectively, which accelerate the flow. This is a continuous energy conversion process where pressure work is converted to axial kinetic energy flux. For the energy balance, Eq. (6), this implies that the distribution between the pressure work and axial kinetic energy flux terms will be dependent on the location of the upstream and downstream control volume boundaries.

The combined pressure work and axial kinetic energy flux term consists of both useful thrust generation and loss components. For a propeller operating in open water this division can be explained through the use of a control volume analysis of both linear momentum and energy, in the manner of Drela (2009). For a propeller in open water, consider a control volume enclosing the propeller, the upstream boundary is located far upstream so that the inlet conditions can be considered homogeneous, with advance velocity ($V_A$), no tangential flows and $p_\infty$, and the lateral boundaries are streamlines where $p = p_\infty$. For such a control volume the evaluation can be limited to the control volume downstream boundary (*out*) through definition of velocity and pressure perturbations, $\Delta V_x = V_x - V_A$ and $\Delta p = p - p_\infty$. A control volume analysis of linear momentum provides us with the useful thrust;

$$F_x = \int_{out}(\Delta p + (V_A + \Delta V_x)\rho\Delta V_x)dA. \tag{7}$$

Through multiplication of all momentum flux balance terms with the advance velocity, the thrust power is obtained,

$$P_x = F_x V_A = \int_{out}\left(V_A\Delta p + \rho V_A^2\Delta V_x + \rho V_A(\Delta V_x)^2\right)dA. \tag{8}$$

Performing a control volume analysis of energy for the same control volume gives us the required delivered power expressed as a sum of energy fluxes (similar to Eq. (6)),

$$P_D = \int_{out}\left(\Delta p\Delta V_x + V_A\Delta p + \rho V_A^2\Delta V_x + \rho V_A(\Delta V_x)^2 + \frac{1}{2}\rho(\Delta V_x)^2 V_x\right)dA + \int_{out}\left(\frac{1}{2}\left(V_t^2 + V_r^2\right) + \Delta\widehat{u} + \Delta k\right)\rho V_x dA. \tag{9}$$

$\Delta\widehat{u}$ and $\Delta k$ denotes the change over the control volume in internal and turbulent kinetic energy, respectively. Amongst the pressure and axial kinetic energy flux terms in the energy balance, the thrust power can be identified as well as two additional terms, denoted the secondary axial kinetic energy flux,

$$\int_{out}\frac{1}{2}\rho(\Delta V_x)^2 V_x dA, \tag{10}$$

and the pressure defect work rate,

$$\int_{out}\Delta p\Delta V_x dA. \tag{11}$$

These terms represents the total irreversible outflow losses of pressure work and axial kinetic energy flux through the control volume outlet boundary. They correspond to the total dissipation of pressure work and axial kinetic energy flux to internal energy which eventually occurs downstream due to the mixing out of spatial wake non-uniformity.

Note that the evaluation of secondary axial kinetic energy flux and pressure defect work rate is not possible for the general control volume as described in Fig. 1, since the lateral boundaries are not streamlines with $p = p_\infty$ and the inlet conditions are not required to be homogeneous. For a propeller operating in open water applying an arbitrary control volume with boundaries in the vicinity of the propeller, these two terms can however be evaluated indirectly as the difference between the sum of axial kinetic energy flux plus pressure work and the thrust power evaluated from forces acting on the propeller. This will be shown in Section 4.2.

### 2.2. Transverse kinetic energy flux

Transverse kinetic energy flux is defined as kinetic energy flux in directions other than the vessel sailing direction. Transverse kinetic energy is often associated with radial and tangential flows induced by the propulsion unit, but can for instance also be due to a propeller slipstream not in line with the sailing direction or bilge vortices caused by the hull curvature.

Transverse kinetic energy flux behind the propulsion unit or vessel should be considered as a loss since the accelerated water in a direction other than the course of the vessel will not contribute to useful thrust. Note that, dependent on application and control volume, it can also appear as a negative term, i.e. as a gain, when the transverse kinetic energy inflow is exceeding the outflow from the control volume.

### 2.3. Internal energy and turbulent kinetic energy flux

In a viscous flow, kinetic energy of the mean flow is converted to internal energy, i.e. heat, through two processes: (A) Dissipation of turbulent velocity fluctuations and (B) direct viscous dissipation from the mean flow to internal energy. Thus, the internal energy flux is a measure of both these processes, whereas the turbulent kinetic energy flux only accounts for an intermediate stage in (A). The turbulent kinetic energy has to be included only due to the CFD modeling, where turbulence is modeled using an eddy-viscosity model. There is actually no need to study the internal energy and turbulent kinetic energy fluxes separately since they both are due to the same phenomena, kinetic energy losses due to turbulence and fluid viscosity in boundary layers and elsewhere where spatial non-uniformities mix out.

The internal energy is obtained through $\widehat{u} = c_p T$ ($c_p$ = specific heat capacity, $T$ = temperature), i.e. a temperature field is required from CFD, implying that the energy equation needs to be solved for. Note that the temperature increase due to dissipation is very small, requiring well-resolved CFD results to obtain sufficient accuracy.

Internal and turbulent kinetic energy can be considered as pure losses. The viscous losses are highly dependent on the velocity of the propeller blade relative to the surrounding water, flow separations and the existence of spatial non-uniformities in the flow that will be mixed out, such as circumferential variations associated with the finite number of blades and flow structures, such as hub/tip vortices and wakes.

## 3. CFD simulation of propeller in open water

A model scale (1:22.629) propeller tested at MARINTEK, Trondheim, has been used for the analyses. It is a four-bladed propeller designed for a 120 m single-screw cargo vessel with a propeller diameter ($D_P$) of 185.6 mm, pitch ratio (at r/R = 0.7) of 0.975 and a blade area ratio of 0.515. For validation purposes, advance ratios (J) between 0.1 and 0.9 are simulated. However, to limit the extent of the energy balance analysis it is only conducted at J = 0.65, which is close to the best efficiency point of the propeller. The simulated propeller rotation rate is 11.32 rps,

identical to open water test conditions.

### 3.1. Computational domain

The computational domain is divided into one outer stationary domain and one inner propeller domain. The stationary domain is extending $10D_P$ upstream and downstream the propeller and $20D_P$ in diameter. The propeller is placed on a streamlined cylindrical body, to mimic the boundary layers close to the propeller hub during model tests, see Fig. 2. To avoid interpolation errors on periodic boundaries a full propeller is studied.

The computational grids are generated in STAR-CCM + v10.06. Polyhedral cells, which are suitable for geometries with highly curved surfaces, are employed inside the propeller domain. Prism layers are extruded from the polyhedral surface mesh using the advancing layer mesher in STAR-CCM+. The boundary layers are resolved, using 15 prism layers near the walls with an expansion ratio of 1.3, see Table 1 for resulting $y^+$ -values. Similar to common practice for self-propulsion simulations, the outer domain consists of cut-cells, which are predominantly hexahedral cells, created using the Trimmer mesher in STAR-CCM+. The mesh structure within the propeller region is shown in Fig. 3. The applied meshing strategy is similar to the one applied by Andersson et al. (2015), where for instance leading/trailing edge refinement, surface cell size and the effect of switching between wall functions and resolved boundary layers were studied. Here, only the overall mesh refinement is studied to evaluate its influence on the results such as the delivered power and the energy flux components through the control volume.

### 3.2. CFD simulation method

The commercial CFD package STAR-CCM + v10.06, a finite volume method solver, is employed. STAR-CCM+ is a general purpose CFD code used for a wide variety of applications. It solves the conservation equations for momentum, mass, energy, and turbulence quantities using a segregated solver based on the SIMPLE-algorithm. A second order upwind discretization scheme in space is used. In addition to the standard procedure for open water propeller simulation, the energy equation is also solved. This enables the measurement of kinetic and turbulent kinetic energy dissipation in the form of a temperature rise.

Since the main aim of the energy balance analysis is to study propeller hull interaction, a turbulence model suitable for these kind of applications is applied also for the propeller open water simulations. Thus, turbulence is modeled using k-$\omega$ SST, which in previous studies has been considered as a reliable compromise for self-propulsion simulations with free-water surface (Andersson et al., 2015). The effect of employing $\gamma - Re_\Theta$ transition model (Menter et al., 2004) along with k-$\omega$ SST will be studied in Section 3.4. Since the transition model is sensitive to turbulent intensity and turbulent viscosity ratio, to counteract the decay of turbulence from inlet boundary to propeller, the method outlined by Bhattacharyya et al. (2015) will be applied. When the transition model is applied the grid is adjusted to better suit the model requirements. This implies a refined grid on the propeller blade in $x^+$ and $z^+$ directions and reduced expansion ratio to 1.2, while the total prism layer thickness is kept unmodified. These changes leads to about 50% increase in the propeller domain cell count.

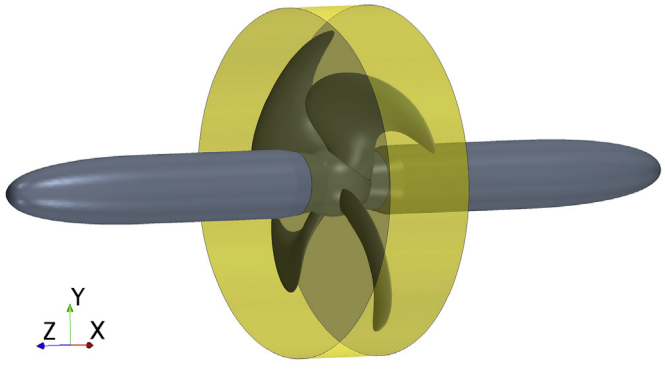


**Fig. 2.** Propeller geometry attached to a streamlined cylindrical body. Interface between propeller and outer domain shown in yellow. (For interpretation of the references to color in this figure legend, the reader is referred to the Web version of this article.)

**Table 1**
Grid data and results for grid convergence study at J = 0.65.

| | Grid 1 | Grid 2 | Grid 3 |
|---|---|---|---|
| Cells in total | $8.25{\cdot}10^6$ | $16.76{\cdot}10^6$ | $41.76{\cdot}10^6$ |
| Cells, prop. domain | $5.77{\cdot}10^6$ | $8.65{\cdot}10^6$ | $15.92{\cdot}10^6$ |
| Cell base size | 5.25 mm | 3.5 mm | 2.33 mm |
| Average $y^+$ on blade | 1.42 | 0.95 | 0.63 |
| Max $y^+$ on blade | 5.47 | 3.99 | 3.00 |
| $K_T$ | 0.180 | 0.180 | 0.179 |
| $K_Q$ | 0.0306 | 0.0304 | 0.0303 |
| Efficiency, $\eta$ | 60.8% | 61.1% | 61.2% |

The advance velocity is set on the inlet boundary to reach the desired operating point. Moreover, the turbulence intensity and the turbulence viscosity ratio are set to 1% and 10, respectively. On the outlet boundary a static pressure is prescribed, while the far field lateral boundary is modeled as a symmetry plane. Multiple reference frames (MRF) are applied, where a rotating reference frame is specified for the propeller domain and a stationary reference frame for the outer domain.

Convergence is measured through average residuals as well as averaged quantities such as thrust and torque. A simulation is considered converged when the residuals are stable and averaged quantities are stable and deviating with less than ±0.1% from their mean value.

### 3.3. Grid convergence

Three grids with a cell refinement ratio of 50% are generated, see Table 1 for details. The thrust coefficient ($K_T = thrust/(\rho n^2 D_P^4)$) scatters within 0.3% between the grids and the torque coefficient ($K_Q = torque/(\rho n^2 D_P^5)$) decreases with increased mesh refinement, resulting in a 0.9% difference between Grid 1 and 3. The maximum difference in efficiency ($\eta = thrust{\cdot}V_A/P_D$) is 0.4 %-points among the grids. Despite that a clear mesh convergence cannot be observed, the small differences between the grids indicate that the resolution is sufficient to represent the main flow features.

### 3.4. Validation

CFD results applying k-$\omega$ SST with and without $\gamma - Re_\Theta$ transition model are compared to open water test data in Fig. 4. Grid 2 and a transition-model-adapted version of Grid 2 are used accordingly.

As shown in Fig. 4, the computed thrust and torque are under estimated compared to experiment, apart from at high advance ratios. The prediction of thrust and torque is improved by applying the transition model, indicating that the Reynolds number during test most probably has been too low to create a fully turbulent flow over the entire blade surfaces. The correspondence between CFD results and open water test data is slightly lower than expected. Accurate CFD results are crucial for the outcome of the energy balance analysis, therefore more effort in general needs to be spent on obtaining accurate CFD methods representative for model as well as full scale conditions. However, the ambition here was not to reproduce the experiments, but rather to conduct a standardized CFD-simulation of a propeller in open water. Further, the detailed test conditions and procedures are unfamiliar to the authors and due to the relatively low Reynolds number of the tests, the flow transition from laminar to turbulent will substantially influence the results.

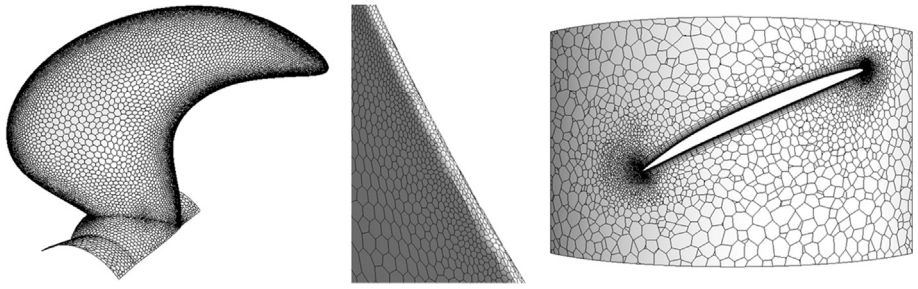

**Fig. 3.** Propeller domain grid (Grid 2). Surface grid, a close up of the trailing edge resolution and a cylindrical cut through at 70% propeller radius.

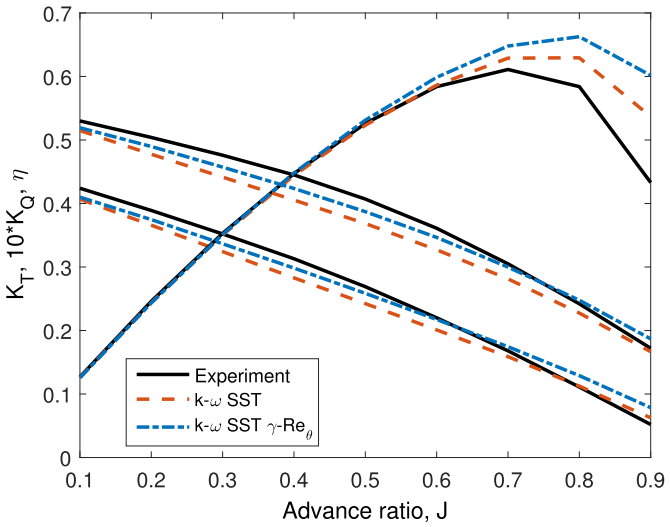


**Fig. 4.** CFD results in terms of $K_T$, $K_Q$ and $\eta$ compared to open water test data.

## 4. Energy balance analysis of propeller in open water

The energy balance analysis is applied on the studied propeller in open water. The work done by viscous stresses on the control volume surface is investigated further in Section 4.1. Thereafter the influence of size/location of the control volume and grid refinement on the energy balance analysis is demonstrated in Section 4.2 and 4.3, respectively. Finally the energy balance analysis is discussed together with qualitative results in Section 4.4.

The control volumes are established as a post-processing step, with the aid of extracted surfaces (using "derived parts" in STAR-CCM+), to enable flexibility when analyzing the results. The control volume boundaries are all located within the outer domain, consisting of a cut-cell grid aligned with a Cartesian coordinate system. To avoid unnecessary interpolation, the shape of the control volumes within this study is set to a rectangular box, aligned with the same coordinate system as the grid.

### 4.1. Work by viscous stresses on control volume surfaces

The work performed by viscous stresses on control volume surfaces, shown in Eq. (3), is at its maximum if the control volume surfaces are placed tangential to the flow direction and there are significant velocity gradients within the flow. If the flow is approximately normal to the control volume surface or if they are placed outside the boundary layer, viscous stresses are expected to be lower.

The work performed by viscous stresses is evaluated on two different control volumes, both with upstream and downstream boundaries located at $0.5D_P$ from the propeller, while the lateral boundaries are located at $1.02D_P$ and $1.5D_P$ from the propeller center, respectively.

For both control volumes the work performed by viscous stresses is negligible, constituting less than 0.01% of the propeller power. The lateral boundaries of both control volumes are located in areas with predominantly low velocity gradients. The largest share of the work performed by the viscous stresses on these control volumes, is due to tangential flow and strong velocity gradients on the control volume downstream boundary.

Since it may not be possible to obtain suitable control volume boundary locations for more complex cases, avoiding areas with tangential flow and significant velocity gradients, it is recommended to always include an evaluation of the work performed by viscous stresses.

### 4.2. Influence of control volume

The energy balance analysis is conducted over two different control volumes, denoted A and B, illustrated in Fig. 5. The upstream and downstream boundaries are located at $0.5D_P$ and $5D_P$ from the propeller center for control volume A and B, respectively. The lateral boundaries are located at $1.5D_P$ from the propeller center for both control volumes. The energy balance for control volume A and B, based on the results for Grid 2, is shown in Fig. 6 and the detailed numbers are provided in Table 2. The propeller thrust power is based on the forces acting on the propeller, and the axial wake non-uniformity loss is calculated as the difference between axial kinetic energy flux/pressure work and the thrust power. This implies that the axial wake non-uniformity loss represents the secondary axial kinetic energy flux (Eq. (7)) and pressure defect work rate (Eq. (8)).

The internal and turbulent kinetic energy flux is larger for control volume B than for A. This is explained by turbulent and viscous dissipation due to mixing out of spatial non-uniformities, occurring between $0.5D_P$ and $5D_P$ downstream of the propeller, within the propeller slipstream as well as on the border between the slipstream and surrounding water. This is also observed through a reduction in the axial wake non-uniformity loss term for control volume B, relative to control volume A. This shows that for a representative illustration of the axial wake non-uniformity loss, the control volume downstream boundary has to be located in the vicinity of the propeller.

The transverse kinetic energy flux is increased for control volume B, which may be surprising, since the main energy conversion process ought to be from kinetic energy to internal and turbulent kinetic energy. This is however not just a study including a propeller, but also the cylindrical body attached to the propeller. This implies that control volume B will capture the hub vortex leaving the cylindrical body, while control volume A will not.

A slightly larger discrepancy between delivered power and the energy balance is observed for the larger control volume, B, compared to A, as shown on the last line in Table 2; this will be discussed further in Section 4.3.

The energy balance for control volumes with different locations of the downstream boundary is shown in Fig. 7, with the upstream boundary kept constant at a distance of $0.5D_P$ from the propeller and the lateral boundaries at $1.5D_P$. In this figure the pressure work and axial kinetic

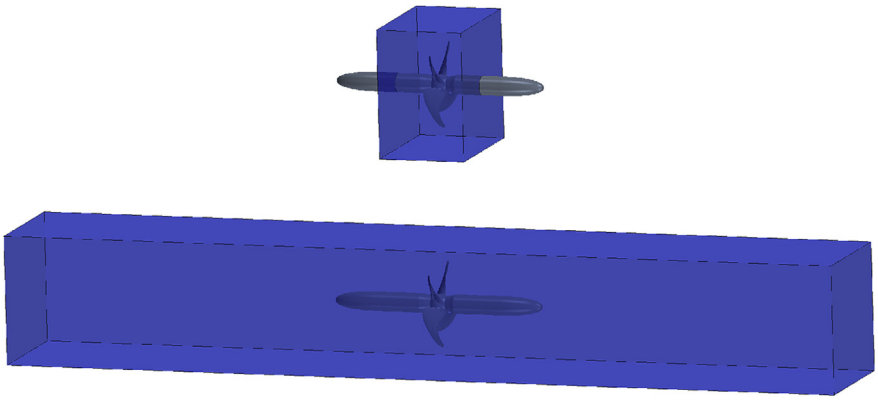

**Fig. 5.** Control volume A (top) and B (bottom).

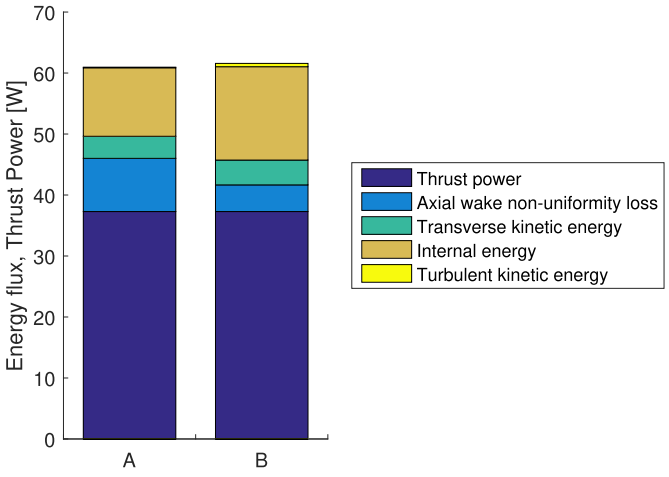


**Fig. 6.** Energy balance for control volume A and B (detailed data available in Table 2).

**Table 2**
Energy balance for propeller in open water (Grid 2).

| | Control volume A | Control volume B |
|---|---|---|
| Thrust power | 37.29 (61%) | 37.29 (61%) |
| Axial wake non-uniformity loss | 8.72 (14%) | 4.37 (7%) |
| Transverse kinetic energy flux | 3.62 (6%) | 4.07 (7%) |
| Internal energy flux | 11.23 (18%) | 15.31 (25%) |
| Turbulent kinetic energy flux | 0.10 (0.2%) | 0.54 (0.9%) |
| Sum energy balance | 60.96 | 61.58 |
| Propeller power, $P_D$ | 61.02 | 61.02 |
| *Difference* | *−0.08%* | *0.93%* |

energy flux terms are kept separate, without indication of the axial wake non-uniformity loss term. The axial deceleration of the flow and appearance of a hub vortex behind the cylindrical body, ending at $\sim 1.25D_P$, influences the evolution of the axial kinetic energy flux, pressure work and transverse kinetic energy flux terms. The contribution from the pressure work term to the energy balance is larger the closer the downstream boundary is located to the propeller, while the opposite holds for the axial kinetic energy flux; a behavior which is in accordance with common actuator disc theory. The internal and turbulent kinetic energy fluxes increase as the downstream boundary is moved away from the propeller, due to viscous and turbulent dissipation associated with mixing out of spatial non-uniformities in the flow. The conversion process from kinetic energy to internal energy will in theory continue until

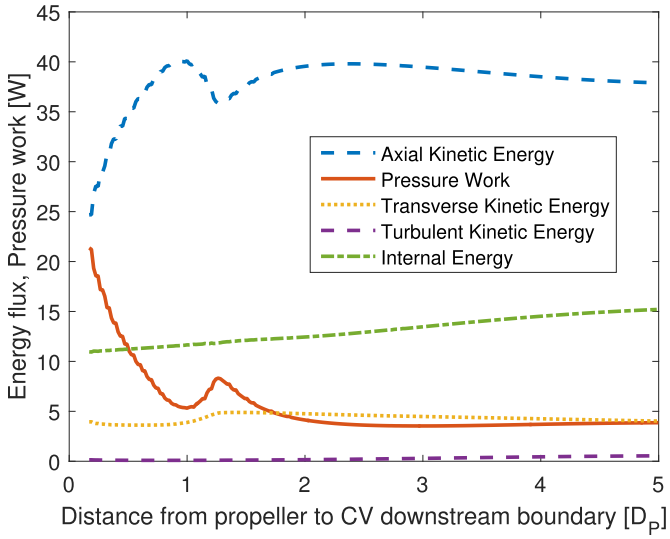


**Fig. 7.** Energy balance components against the location of the downstream control volume surface based on Grid 2. Upstream and lateral boundaries are placed $0.5D_P$ and $1.5D_P$ away from the propeller center, respectively.

all energy has been dissipated into heat further downstream.

As discussed above, the control volume choice has an important role on the energy balance results. Obviously more information about the flow is obtained in the vicinity of the propulsion unit, whereas further away the kinetic energy terms are to a larger extent converted to internal and turbulent kinetic energy. Since the distribution of the energy balance is highly dependent on the location of the control volume, it is important to apply identical control volumes when comparing different designs.

### 4.3. Accuracy and influence of grid refinement

It was noted in Section 4.2 that a better agreement between the delivered power, evaluated based on forces acting on the propeller, and energy balance was obtained for the smaller control volume (A). In Fig. 8 the difference between these terms is compared for different control volumes, were the upstream and lateral boundaries are fixed while the position of the downstream boundary is varied. Until the end of the cylindrical body at $\sim 1.25D_P$, the difference oscillates around zero. This is most probably associated with inaccuracies in the numerical convergence of the solution and interpolation errors on the control volume surfaces. Behind the cylindrical body, the difference increases with increasing distance between propeller and downstream boundary, and reaches $\sim$ 0.8% of the delivered power at $5D_P$, which most probably is associated with numerical dissipation.

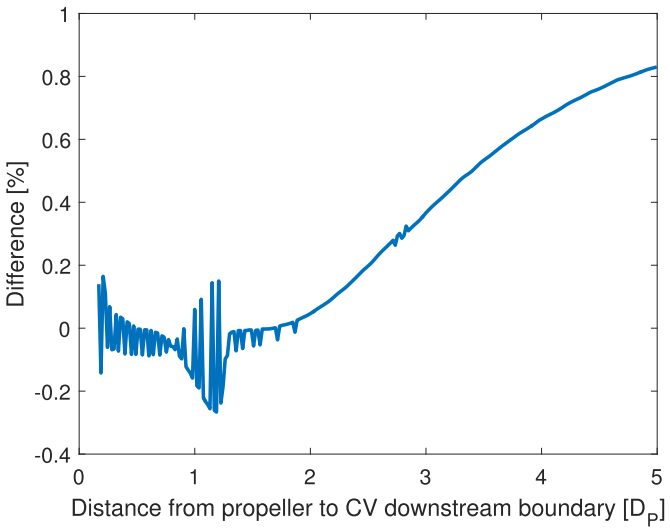


**Fig. 8.** Difference between energy balance evaluated over control volume and propeller power. Downstream boundary of control volume moved, while upstream boundary is fixed at $0.5D_P$ and lateral boundaries at $1.5D_P$ from propeller center. Based on Grid 2.

In Table 3 the energy balance analysis is conducted using control volume A on Grid 1, 2 and 3, respectively. The difference between the energy balance and the delivered power, evaluated based on forces acting on the propeller, is below 0.3% for all grids. The difference does not decrease with increasing grid refinement. However, relating to Fig. 8, the magnitude of the oscillations, most probably related to inaccuracies in the numerical convergence of the solution and interpolation errors on the control volume surfaces, is reduced with increased grid refinement. Interestingly, the differences between the energy balance between Grid 1, 2 and 3 are less than the differences between the delivered power. The discrepancies are most probably deduced from a combination of numerical dissipation and numerical convergence of solution.

Table 3 also includes the detailed energy balance decomposition. The pressure work reduces with increased grid refinement, while the axial kinetic energy flux contribution increases. Studying these terms combined, which often is relevant, less difference is seen between the grids, 75.0%, 75.5% and 76.0%, respectively. A larger contribution from these terms and the transverse kinetic energy flux, in conjunction with grid refinement, can be related to the reduced contribution from internal energy flux. A finer grid may imply a reduced numerical dissipation in the propeller vicinity.

To estimate the level of numerical dissipation for control volume A, a Rickardson extrapolation of the internal energy flux is conducted, see Fig. 9. Two additional grids, coarser than Grid 1 (still keeping the cell refinement ratio of 50%), are included for the extrapolation. Due to the unstructured grid, a Rickardson extrapolation is not strictly valid, but can still give an indication of the discretization error. The discretization error

**Table 3**
Energy balance for propeller in open water, applying control volume A on Grid 1, 2 and 3.

| | Grid 1 | Grid 2 | Grid 3 |
|---|---|---|---|
| Axial kinetic energy flux | 34.15 (55.8%) | 34.67 (56.9%) | 35.41 (58.1%) |
| Pressure work | 11.75 (19.2%) | 11.34 (18.6%) | 10.90 (17.9%) |
| Transverse kinetic energy flux | 3.56 (5.8%) | 3.62 (5.9%) | 3.75 (6.2%) |
| Internal energy flux | 11.61 (19.0%) | 11.23 (18.4%) | 10.77 (17.7%) |
| Turbulent kinetic energy flux | 0.11 (0.2%) | 0.10 (0.2%) | 0.10 (0.2%) |
| Sum energy balance | 61.17 | 60.96 | 60.93 |
| Propeller power | 61.30 | 61.02 | 60.76 |
| *Difference* | *−0.20%* | *−0.08%* | *0.29%* |

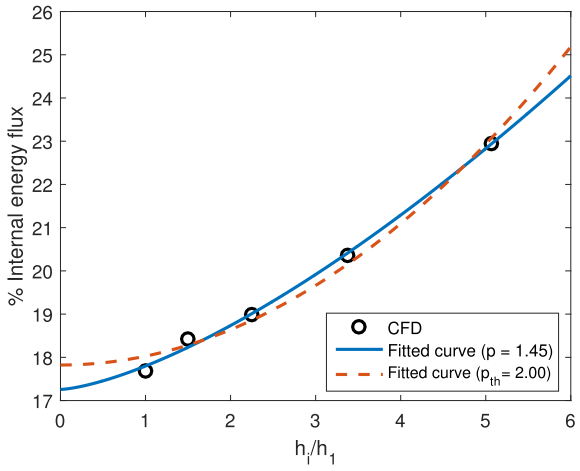


**Fig. 9.** Rickardson extrapolation of the internal energy flux, shown as the share of the total energy balance for control volume A.

of the internal energy flux may be considered as a representative of the numerical dissipation. The error is 1.2% for control volume A and Grid 2, in comparison to the asymptotic value of the internal energy flux, 17.3%.

Since the energy decomposition is grid dependent, it is highly recommended to apply similar meshing strategy and grid refinement level for comparative studies.

### 4.4. Discussion

To be able to improve the propulsive system, or to analyze differences in performance between propulsive systems, the energy balance decomposition is preferably complemented by a visualization of the energy fluxes. In Fig. 10, the internal energy flux is shown over the control volume surface. As expected, the flux is negligible on the upstream and lateral control volume boundaries where no work has been extracted from the flow. On the downstream side of the control volume, the boundary layer losses from the individual blades are depicted. The highest level of internal energy flux is seen in the tip region, where the blade velocity relative the surrounding fluid is highest and the tip vortex is present. For a ship propulsion system, including skeg, propeller axes, rudder etc, it can be beneficial to view all sides of this volume, as well as intermediate surfaces within the control volume to be able to analyze and locate the origin of the losses.

Due to the absence of interaction effects for the propeller in open water, the visualization of the results is limited to contour plots of axial kinetic energy flux, transverse kinetic energy flux, pressure work and internal energy flux at a distance of $0.2D_P$ downstream the propeller, see Figure 11. Note that the color scales are different for the different terms, so direct comparisons should not be made.

The high pressure produced behind the blade surfaces is clearly depicted at this distance behind the propeller. The circumferential non-uniformities due to the four blades are also observed on the axial kinetic energy flux contour plot. The axial wake non-uniformity loss (secondary axial kinetic energy flux and pressure defect work rate) are not visualized since they cannot be evaluated for a generic control volume. These terms will however decrease as the pressure and axial velocity perturbations are reduced and the relative magnitude of the perturbations between different designs may be identified with the aid of axial kinetic energy flux and pressure work contour plots.

The transverse kinetic energy originates from the wake behind the propeller blade, with the highest fluxes initiate from the propeller root, where suction side separation zones are present.

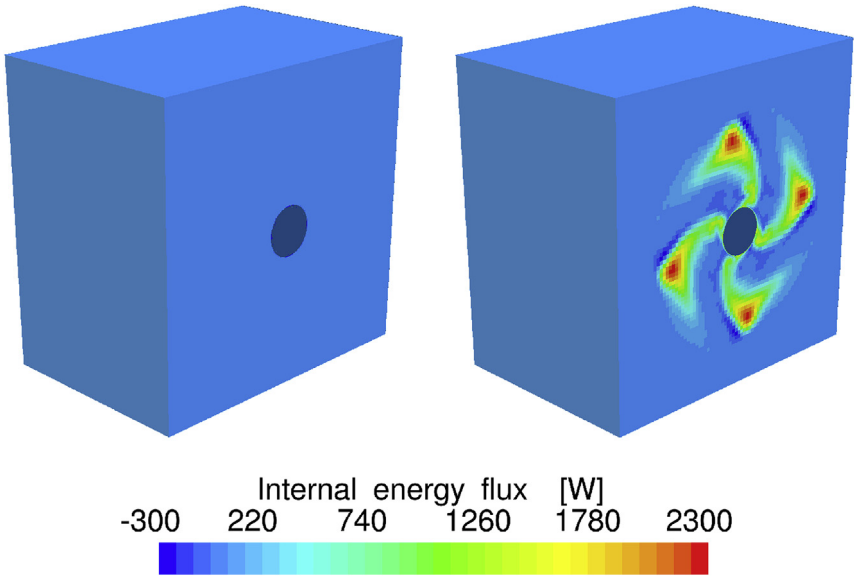


**Fig. 10.** Contours of internal energy flux on control volume A viewed from upstream (left) and downstream (right).

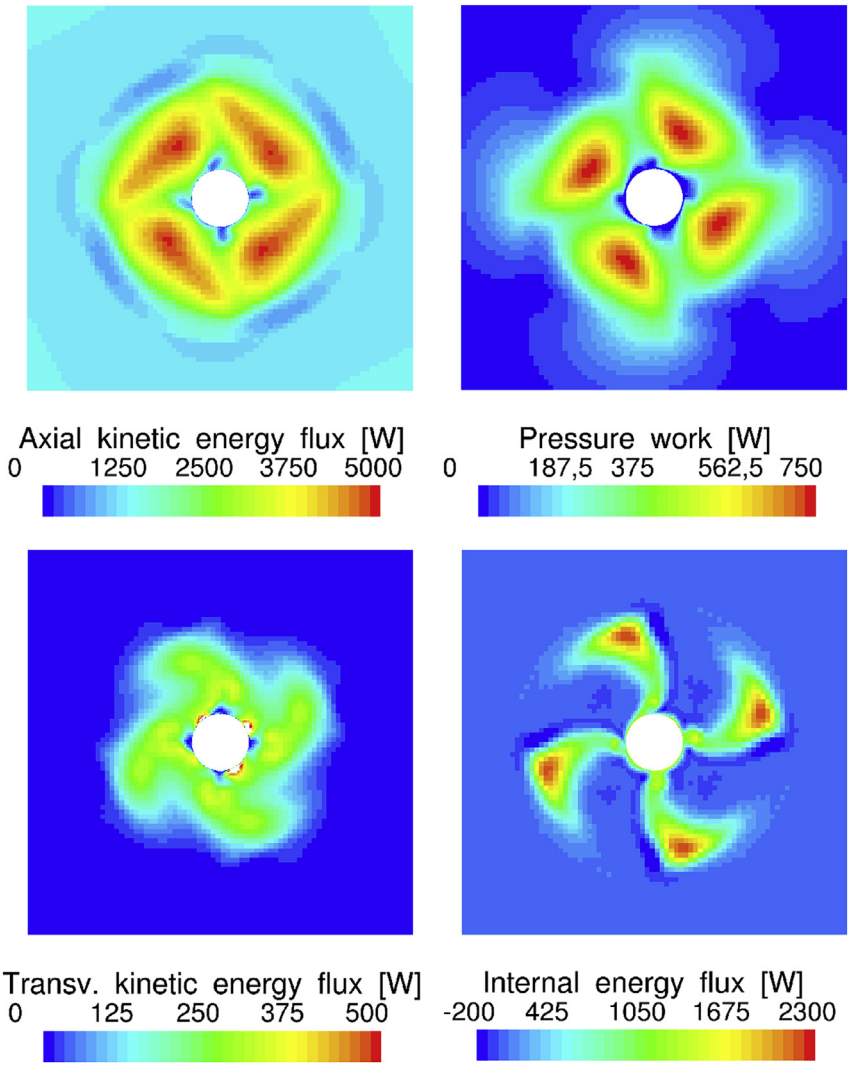


**Fig 11.** : Contours of Axial kinetic energy flux, pressure work, transverse kinetic energy flux and internal energy flux at $0.2D_P$ downstream the propeller.

## 5. Conclusions

We have shown that a control volume analysis of energy applied on CFD results provide an alternative method to study the power consumption of a propulsion unit. The delivered power to the propeller shaft can be expressed in terms of thrust power, axial wake non-uniformity losses, transverse kinetic energy flux and internal/turbulent kinetic energy flux. This implies that the hydrodynamic losses associated with a high and/or uneven acceleration of the flow, slipstream rotation and viscous losses can be tracked and quantified. Since all possible hydrodynamic losses in the system are depicted in the analysis it should be possible for a designer to avoid sub-optimized solutions.

We consider this method promising, as a complement to the established methods based on experimental procedures, for analyzing propulsor hull interaction. Especially for novel, but also for more common, propulsion configurations where the hydrodynamic performance cannot always be fully understood based on established methods. The method also enables analysis of the propeller performance during one revolution, which can open up possibilities for design improvements. Our further work will therefore focus on application of the energy balance analysis on propulsion systems in behind conditions as well as a quantitative method for determination, or guidance, of the distribution between favorable and loss components of axial kinetic energy flux/pressure work for more complex systems.

Energy balance analyses can be used not only as a tool for more comprehensive understanding of a system, but it can also be used within design and automated optimization procedures since it gives quantitative information on the hydrodynamic losses. It is a post-processing tool with the only additional requirement of solving the energy equation, and can be employed in any CFD-code based on commonly available variables.

## Acknowledgements

This research is supported by the Swedish Energy Agency (grant number 38849-1) and Rolls-Royce Marine through the University Technology Centre in Computational Hydrodynamics hosted by the Department of Mechanics and Maritime Sciences at Chalmers. The simulations were performed on resources at Chalmers Centre for Computational Science and Engineering (C3SE) provided by the Swedish National Infrastructure for Computing (SNIC).

## References

Andersson, J., Hyensjö, M., Eslamdoost, A., Bensow, R., 2015. CFD simulations of the Japan bulk Carrier test case. In: Proceedings of the 18th Numerical Towing Tank Symposium. Cortona, Italy.

Bhattacharyya, A., Neitzel, J.C., Steen, S., Abdel-maksoud, M., Krasilnikov, V., 2015. Influence of flow transition on open and ducted propeller characteristics. In: Proceedings of the Fourth International Symposium on Marine Propulsors. (Austin, Texas, USA).

Capitao Patrao, A., Avellán, R., Lundbladh, A., Grönstedt, T., 2016. Wake and loss analysis for a double bladed swept propeller. In: Proceedings of ASME Turbo Expo 2016. Seoul, South Korea.

Dang, J., Dong, G., Chen, H., 2012. An exploratory study on the working principles of energy saving devices (ESDS) - PIV, CFD investigations and ESD design guidelines. In: Proceedings of the ASME 2012 31st International Conferecen on Ocean, Offshore and Arctic Engineering OMAE2012. Rio de Janeiro, Brazil.

Dang, J., Hao, C., Rueda, L., Willemsen, H., 2015. Integrated design of asymmetric aftbody and propeller for an aframax tanker to maximize energy efficiency. In: Proceedings of the Fourth International Symposium on Marine Propulsors. (Austin, Texas, USA).

Denton, J.D., 1993. The 1993 IGTI scholar lecture loss mechanisms in turbomachines. J. Turbomach. 115, 621–656.

Drela, M., 2009. Power balance in aerodynamic flows. AIAA 47 (7), 1761–1771.

Dyne, G., 1995. The principles of propulsion optimization. In: Trans. RINA 137. London, United Kingdom.

Menter, F.R., Langtry, R.B., Likki, S.R., Suzen, Y.B., Huang, P.G., Völker, S., 2004. A correlation-based transition model using local VariablesPart I: model formulation. J. Turbomach. 128 (3), 413–422.

Schuiling, B., van Terwisga, T., 2016. Energy analysis of a propeller in open water using a RANS method. In: 24th International HISWA Symposium on Yacht Design and Yacht Construction. Amsterdam, The Netherlands.

van Terwisga, T., 2013. On the working principles of energy saving devices. In: Proceedings of the Third International Symposium on Marine Propulsors. Launceston, Tasmania, Austrailia.

White, F.M., 2008. In: Fluid Mechanics, sixth ed. McGraw-Hill, New York.